JOURNAL OF GUIDANCE, CONTROL, AND DYNAMICS
Vol. 30, No. 5, September–October 2007

Engineering Notes

ENGINEERING NOTES are short manuscripts describing new developments or important results of a preliminary nature. These Notes should not exceed 2500 words (where a figure or table counts as 200 words). Following informal review by the Editors, they may be published within a few months of the date of receipt. Style requirements are the same as for regular contributions (see inside back cover).

Robust Decentralized Fault Detection in Leader-to-Follower Formations of Uncertain Linearly Parameterized Systems

Nicolas Léchevin* and Camille Alain Rabbath†
Defence Research and Development Canada—Valcartier, Québec, Québec G3J 1X5, Canada

DOI: 10.2514/1.27938

I. Introduction

FAULT/FAILURE detection, isolation, and recovery (FDIR) methods are usually designed for flight-critical components such as actuators and sensors, using detailed mathematical models. See, for instance, [1] and references therein for recent results. Although component-level FDIR (CL-FDIR) has led to convincing results for the individual unmanned aerial vehicle (UAV), much remains to be done for leader-to-follower formations. Indeed, from the distributed nature of formation guidance laws, when a CL-FDIR cannot preserve flight performance for certain faults or failures, an abnormal behavior arising in a single vehicle can potentially lead to formation instability. We therefore claim that there is a need for a decentralized fault detection (DFD) and adaptation capability so that each vehicle can detect anomalous behaviors in neighboring vehicles and adapt its own guidance law accordingly.

To the best of our knowledge, there is no work reported to date in the literature that proposes the technology to handle concurrent component-level faults and information-flow faults. However, the particular case of formation reconfiguration under information-flow faults has been studied by a few researchers. UAV formation reconfiguration strategies are proposed in [2–4] based on graph theory and a modified Dijkstra algorithm to command geometry changes and to optimally reconfigure communication channels once information-flow faults have been detected. From another perspective, [5] proposed an interacting-multiple-model FDIR approach for formations faced with communications failure.

In this paper, we propose a DFD technique to address worst-case situations involving concurrent communications loss and component faults for leader-to-follower formations. Because the state of the formation cannot be published across the network at the time of faults, sensory data onboard UAVs are used by the observer. Each vehicle of the formation computes residues associated with the position of its neighbors. A neighbor j of vehicle i refers to a vehicle for which the separation from i is less than or equal to the sensor range of vehicle i. Each residue is obtained from a robust observer based on the use of a simplified, uncertain, linearly parameterized model of the neighbor j for which the dynamics is perturbed by exogenous signals. Such signals depend on the state of vehicle k, which is a neighbor of j but not necessarily of i. Vehicle i estimates these exogenous signals by low-pass filtering the inverse of vehicle j's dynamics, which is assumed to be the minimum phase. An observer designed from H_∞ gain-based minimization provides vehicle i with residues that characterize the state of j, while reducing the impact of modeling uncertainties. The effectiveness of the proposed DFD technique is demonstrated with the distributed formation controller of [6,7]. The simulation results shown in this paper rely on high-fidelity, fully nonlinear, 6-DOF, sampled-data, aerial almost-lighter-than-air vehicle (ALTAV) models, which include actuator saturation, realistic measurement noise, and commercial off-the-shelf sensor sampling rates.

II. Modeling of Formation, Vehicles, Control, and Faults

A. Formation

Consider a formation of n identical UAVs comprising a single leader and $n-1$ followers. The leader tracks a known reference trajectory. The leader is node 0 and the followers are nodes 1 to $n-1$ of a graph $G = (S, E)$. Graph G is defined by the set of vertices $S = \{0, \ldots n-1\}$ and a set of edges given as $E = \{(i, j); i, j \in V\}$. Vehicle positions are expressed in inertial frame I_{xyz}. Associate to each node i the set N_i, which includes the ith node and all the neighboring vehicles j in the formation that are sensed by node $i \in V$. N_i is endowed with a neighboring unidirectional relation, in which sensory data (position and velocity of j) flow from $j \in N_i$ to i; that is, $j \in N_i$ implies that i measures the relative distance r_{ij} that separates i from j. The converse is false unless $i \in N_i$. The formation geometry is defined, as shown in Fig. 1, by prescribed angle λ^*_{ij} and relative distances ρ^*_{ij}, assumed time-invariant in this Note. Such information is transmitted from one node to another according to G. For example, the configuration of Fig. 1 displays the formation with j as the leader, i as j's follower ($j \in N_i$), and k as i's follower ($i \in N_k$); k and i measure (r_{ki}, λ_{ki}) and (r_{ij}, λ_{ij}), respectively. In the present setting, no intervehicle communication is required. Data are obtained by means of onboard sensors.

B. Simplified Model of Vehicle Closed-Loop Dynamics

DFD implemented in each vehicle $k \in S$ does not consist of a mere duplication of the CL-FDIR of k's neighboring vehicles. This approach would be computationally cumbersome and would simply reproduce the recovery incapability found with the CL-FDIR. Instead, we propose to develop a simplified state-space representation of neighboring vehicle dynamics in a closed loop with their control law and to base the design of the neighboring vehicle fault detector on this simplified model. Planar decentralized control of a formation of ALTAVs, as that depicted in Fig. 1, serves as the motivational example to demonstrate the effectiveness of the proposed DFD. Indeed, the slow dynamics of the ALTAVs and their smooth degradation of performance when faced with faults make them the ideal unmanned vehicles for the development of a team-level DFD experimental testbed. The detailed closed-loop dynamics

Received 20 September 2006; revision received 23 March 2007; accepted for publication 6 May 2007.

*Visiting Fellow, 2459 Pie-XI North; Nicolas-Lechevin@drdc-rddc.gc.ca.
†Defence Scientist, 2459 Pie-XI North; Camille-Alain.Rabbath@drdc-rddc.gc.ca.

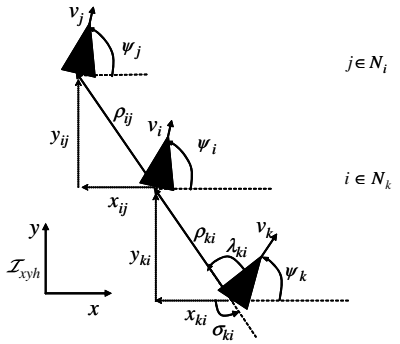

Fig. 1 Geometry of a formation of three vehicles; formation flight control aims at achieving a path following the *x–y* plane; set-point regulation in *z* is obtained by PID control around a prescribed altitude z_t known by all vehicles.

of the formation, as illustrated in Fig. 2a, are described in Appendix A. The ALTAVS are equipped with autopilots and formation guidance laws that ensure path following of the leader vehicle and stabilization of the entire formation around a prescribed geometry.

It is assumed at the DFD level that the behavior of a vehicle is not considered faulty by its neighbors as long as it is able to achieve position trajectory tracking based on measured relative distances regardless of its attitude. The attitude of the 6-DOF model of the vehicle presented in Appendix A is thus not considered in the simplified state-space representation and only the intervehicle's relative distance is used to detect abnormal operating conditions. Recall that detection of mildly abnormal behavior is carried out by the CL-FDIR based on the full 6-DOF nonlinear model.

Therefore, to represent the time-varying flight envelope of ALTAVs $i \in N_k$ and to account for possible bounded parametric uncertainties, the following uncertain linearly parameterized system, shown in Fig. 2b, is proposed:

$$\dot{q}_i = A_i(\alpha_i)q_i + B_i(\alpha_i)\underbrace{\begin{bmatrix} h_i \sum_{j\in N_i} k_i(x_j - x_{ij}^*) \\ h_i \sum_{j\in N_i} k_i(y_j - y_{ij}^*) \\ z_t \end{bmatrix}}_{v_{i1}-v_{i2}} \tag{1}$$

$$\begin{bmatrix} x_i \\ y_i \\ z_i \end{bmatrix} = \begin{bmatrix} 1 & 0 & 0 & 0 & 0 & 0 \\ 0 & 0 & 1 & 0 & 0 & 0 \\ 0 & 0 & 0 & 0 & 0 & 1 \end{bmatrix} q_i$$

where

$$[x_{ij}^* \quad j_{ij}^*]^T = \rho_{ij}^*[\cos(\lambda_{ij}^* + \psi_i)\ \sin(\lambda_{ij}^* + \psi_i)]^T$$

$$q_i = [\,q_{i1} \quad q_{i2} \quad q_{i3} \quad q_{i4} \quad q_{i5} \quad q_{i6}\,]^T$$

x_i, y_i, and z_i are the vehicle translations; ψ_i is the heading angle of vehicle i; and z_t is the prescribed altitude of the formation, which is assumed to be known before the mission. The uncertain parameter α_i is assumed to evolve in the unit simplex:

$$\Gamma_i = \left\{ (\alpha_{i1,\ldots,}\alpha_{is}) \middle| \sum_{j=1}^{s} \alpha_{ij} = 1, \alpha_{ij} \geq 0 \right\}$$

The state-space is assumed linear in α; that is,

$$[A_i(\alpha)|B_i(\alpha)] = \sum_{j=1}^{s} \alpha_{ij}[A_{ij}|B_{ij}]$$

Note that $A_i(\alpha)$ [respectively, $B_i(\alpha)$] can be decomposed as the sum of a nominal matrix $A_i^* = A_i(\alpha^*)$ [respectively, $B_i^* = B_i(\alpha^*)$] and a deviation matrix $\tilde{A}_i(\alpha)$ [respectively, $\tilde{B}_i(\alpha)$] that evolves in the same polytope as that of $A_i(\alpha)$ [respectively, $B_i(\alpha)$]; that is,

$$\tilde{A}_i(\alpha) = \sum_{j=1}^{s} \alpha_{ij}\tilde{A}_{ij}$$

and

$$\tilde{B}_i(\alpha) = \sum_{j=1}^{s} \alpha_{ij}\tilde{B}_{ij}$$

Remark 1:

1) The term $v_{i1} - v_{i2}$ in Eq. (1) results from the distributed controllers of [6,7] applied to vehicle i and its neighbors. Formation stabilization based on distributed controllers presented in Appendix A is guaranteed under the assumption that G is a directed acyclic graph [7]. Furthermore, it is shown input–output stable when faced with exogenous disturbances such as measurement noise and when subject to homothetic morphing commands [6,7].

2) Polytopic interpolation in Eq. (1) has also been used to model the fighter aircraft for the design of fault-tolerant flight control systems in [8].

C. Modeling of Faults

The signal of interest is denoted as $F_i(t)$ and can represent either actuator output signal, control input signal, or an exogenous force, as suggested in Eqs. (A1) and (A2) of Appendix A. Let t_f denote the time at which a fault occurs. $F_i(t)$ can be formally expressed for vehicle $i \in S$ as

$$F_i(t) = K_i[t_f, t, F_{\text{in}}(t)]$$

where $F_{\text{in}}(t)$ denotes the nominal signal, exempt from fault, and K_i is

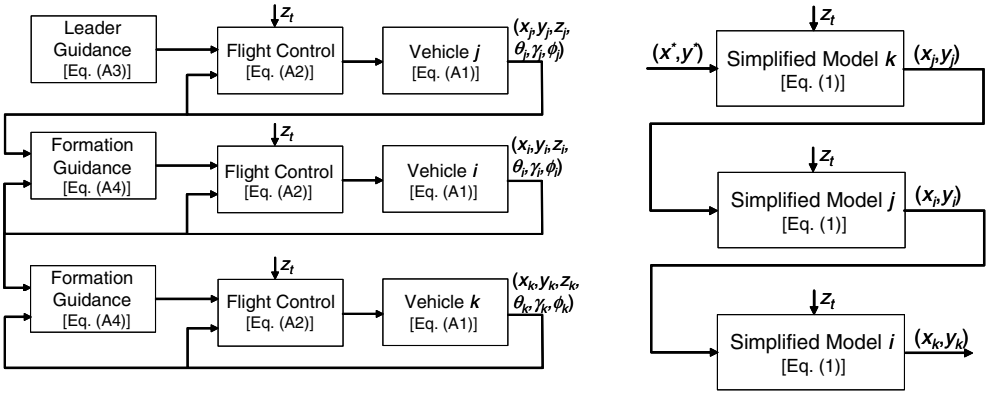

a) Full 6-DOF nonlinear models in closed loop with autopilots and formation guidance laws

b) Simplified linear uncertain representation of the formation

Fig. 2 Representations of formation flight control of vehicles *i*, *j*, and *k*.

the identity function [i.e., $F_i(t) = F_{\text{in}}(t)$] when $t < t_f$ and a polynomial function of F_{in} when $t \geq t_f$. K_i is typically nondifferentiable and even discontinuous at t_f. Because $F_i(t)$ can be expressed as

$$\begin{aligned} F_i(t) &= F_{\text{in}}(t) - F_{\text{in}}(t) + K_i[t_f, t, F_{\text{in}}(t)] \\ &= F_{\text{in}}(t) + 1_{t-t_f}[K_i[t_f, t, F_{\text{in}}(t)] - F_{\text{in}}(t)] \end{aligned} \tag{2}$$

where 1_{t-t_f} is the unit step function, which is equal to 1 if $t \geq t_f$ and to 0, otherwise, vehicle dynamics can be modeled as a closed-loop nominal system excited by disturbance:

$$1_{t-t_f}\{K_i[t_f, t, F_{\text{in}}(t)] - F_{\text{in}}(t)\}$$

Because Eq. (1) is a model simplification of the nominal closed-loop system, uncompensated fault can be represented on the right-hand side of Eq. (1) by means of an additive disturbance δ_i, where faulty signal δ_i belongs to the following set:

$$\begin{aligned} \Omega_\delta = \{&\delta_i \in \Re^3 \backslash \{0,0,0\}; i \in S \backslash \{0\}, \delta_i \\ &= 1_{t-t_f} d_i(t), \|d_i(t)\| \geq D_i > 0 \quad \forall\ t \geq t_f\} \end{aligned} \tag{3}$$

In Eq. (3), entries of d_i are polynomial functions and $D_i > 0$ is a lower bound on the signal d_i such that all faults $\delta \in \Omega_\delta$ are detectable. Conditions about D_i are derived in the next section.

Remark 2:

1) Exogenous disturbance δ_i, which adds to the simplified model, can originate from either an exogenously or endogenously generated fault or failure. For instance, F_{in} involved in actuator failure represents the control signal and thus makes δ_i endogenous to the closed-loop system, although δ_i is not expressed analytically. Furthermore, δ_i may be triggered by an event that is external to the system. Indeed, one can think of a projectile penetrating the body of UAV as one example of the exogenous nature of δ_i.

2) Definition of Ω_δ in Eq. (3) limits the scope of faults to signals characterized by an abrupt jump, which comes from the use in Eqs. (1) and (3) of the unit step function 1_{t-t_f}. The threshold selector used in the DFD and derived in Sec. III.C determines the amplitude of the changes that are detected by the proposed scheme.

3) Incipient faults, such as those resulting from loss of control effector effectiveness or lock-in-place failure [1], do not belong to Ω_δ. For such faults, there is no guarantee of detection by the proposed DFD. Through the numerical simulations, we indeed experienced such detection inability with lock-in-place actuator failures.

III. Synthesis of Fault Detector

A. Observer with Disturbance Compensation

Consider the first-order, linear, time-invariant system

$$\dot{x} = -a(x - \delta - e), \qquad a = a^* + \tilde{a} \tag{4}$$

where $\delta \in \Omega_f$, e is a smooth exogenous signal, and $\tilde{a}$ represents the deviation of parameter a with respect to its nominal value a^*. The objective is to design a detector that is sensitive to the abrupt change δ while attenuating the effect of e.

Denote L and L^{-1} as the Laplace transform and its inverse. The Laplace transform of the time-varying signal $x(t)$ is denoted as $x(s)$. To alleviate the notation, x is understood as $x(t)$.

Using the observer

$$\dot{\hat{x}} = -a^*(\hat{x} - \hat{\delta} - \hat{e}) - L_o\tilde{x} \tag{5}$$

where $\tilde{x} = \hat{x} - x$ and

$$\hat{\delta} + \hat{e} = L^{-1}\left\{\frac{x(s)(s/a^* + 1)}{\tau_f s + 1}\right\} \tag{6}$$

yields the following estimation error dynamics:

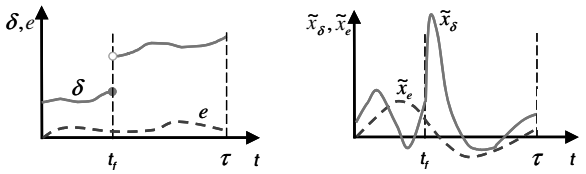

a) Profile of the faulty signal and the exogenous disturbance

b) Estimation error signals

Fig. 3 Observer with compensation of disturbances.

$$\begin{aligned} \tilde{x}(s) = \tilde{x}_\delta(s) + \tilde{x}_e(s) &= \frac{-1}{(s + a^* + L_o)}\left(\frac{a^*\tau_f s}{\tau_f s + 1} + \frac{\tilde{a}s}{s + a}\right) \\ &\times [\delta(s) + e(s)] = H(s)[\delta(s) + e(s)] \end{aligned} \tag{7}$$

From Eq. (7), signal δ is filtered and differentiated. With an appropriate selection of parameters, one can expect the measurement of the error signal $\tilde{x}_\delta$, which is caused by the discontinuous signal δ, to be dominant with respect to that of $\tilde{x}_e$, as suggested by the time-varying signals shown in Fig. 3. It is to be noted that tuning τ_f and L_o results from a tradeoff between a fast detection of δ obtained with small values of τ_f or large values of L_o and maintaining robustness of the estimation with respect to measurement noise.

Adopt the following notation:

$$\Lambda_x(\tau) = \|L^{-1}\{x(s)/s\}\|_\tau \tag{8}$$

where the root mean square (rms), denoted as

$$\|x\|_\tau = \sqrt{1/\tau \int_0^\tau x^T(t)x(t)\,\mathrm{d}t}$$

is used.

Given an upper bound of e ($\|e\|_\tau \leq \bar{e}$), one can compute the lower detectable fault δ (characterized by D) and the corresponding threshold as follows. To avoid false alarms, the threshold is defined by the following inequality:

$$\inf_{\delta \in \Omega, \|e\| \leq \bar{e}} \|\tilde{x}\|_\tau > \sup_{\delta = 0, \|e\| \leq \bar{e}} \|\tilde{x}\|_\tau = J_{\text{th}} \tag{9}$$

The threshold J_{th} is the supremum of the estimation error when no fault occurs; that is, the estimation errors are due only to parametric uncertainty and to the presence of the exogenous signal e. Because, by construction of Ω in Eq. (3), $[0 \quad 0 \quad 0]^T \notin \Omega$, solving Eq. (9) for D provides the minimum detectable fault associated with the system in Eq. (4).

From [9] and the definition of $H(s)$ in Eq. (7), Eq. (9) is satisfied if

$$\inf_{\delta \in \Omega} \|H(s)\delta(s)\|_\tau > 2 \sup_{\|e\| \leq \bar{e}} \|H(s)e(s)\|_\tau \tag{10}$$

from which the following sufficient condition about the minimum detectable fault is obtained:

$$|D| \geq \frac{2\bar{e}\|H(s)\|_\infty}{\Lambda_H(\tau - t_f)} \tag{11}$$

where D is defined in Eq. (3) with $i = 1$. The threshold is thus defined as $J_{\text{th}} = 2\bar{e}\|H(s)\|_\infty$. For the system expressed by Eq. (4) with no parametric uncertainties ($\tilde{a} = 0$), $\Lambda_H(\tau - t_f)$ can be expressed in closed form as

$$\begin{aligned} \Lambda_H(\tau - t_f) &= \sqrt{1/\tau \int_0^\tau [L^{-1}\{H(s)/s\}]^T L^{-1}\{H(s)/s\}\,\mathrm{d}t} \\ &= \frac{a^2\tau_f^2}{\tau(\tau_f(a + L_o) - 1)^2}[e^{-2(a+L_o)(\tau - t_f)} \\ &+ e^{-2(\tau - t_f)} - 2e^{-(a+L_o+1/\tau_f)(\tau - t_f)} - 3]^2 \end{aligned} \tag{12}$$

B. Synthesis of Team-Level Detector

The simplified model in Eq. (1) for $i \in N_k$, which is used by vehicle k to detect faults on neighboring vehicle i, is characterized by the unknown signal x_j, where j is in N_i, but not necessarily in N_k. Considering that signal x^*_{ij} in Eq. (1) is available to k, the following observer is proposed:

$$\begin{cases} \dot{\hat{q}}_i = A_{F,i}\hat{q}_i + B^*_i \underbrace{\begin{bmatrix} h_i \sum_{j\in N_i} k_i(\hat{x}_j - x^*_{ij}) \\ h_i \sum_{j\in N_i} k_i(\hat{y}_j - y^*_{ij}) \\ z_t \end{bmatrix}}_{\hat{v}_{i1} - v_{i2}} + B_{F,i}C_i q_i, \\ r_i = [\,C_i \quad -C_{F,i}\,]\begin{bmatrix} q_i \\ \hat{q}_i \end{bmatrix} \end{cases} \tag{13}$$

where

$$B^*_i \begin{bmatrix} h_i \sum_{j\in N_i} k_i \hat{x}_j \\ h_i \sum_{j\in N_i} k_i \hat{y}_j \\ 0 \end{bmatrix} = L^{-1}\left\{\frac{B^*_i \hat{v}_{i1}(s)}{\tau_f s + 1}\right\} = L^{-1}\left\{\frac{\dot{\bar{q}}_i(s) - A^*_i \bar{q}_i(s) + B^*_i v_{i2}(s)}{\tau_f s + 1}\right\} \tag{14}$$

and

$$\bar{q}_i^{\,T} = \begin{bmatrix} q_{i1} & L^{-1}\left\{\frac{s x_i(s)}{\tau_d s + 1}\right\} & q_{i3} & L^{-1}\left\{\frac{s y_i(s)}{\tau_d s + 1}\right\} & q_{i5} & q_{i6} \end{bmatrix} \tag{15}$$

where $\bar{q}_i$ is given in the time domain.

Furthermore,

$$C_i = \begin{bmatrix} 1 & 0 & 0 & 0 & 0 & 0 \\ 0 & 0 & 1 & 0 & 0 & 0 \end{bmatrix}$$

$$v^T_{i2} = \begin{bmatrix} -h_i \sum_{j\in N_i} k_i x^*_{ij} | - h_i \sum_{j\in N_i} k_i y^*_{ij} | z_t \end{bmatrix}$$

and $q_i = \bar{q}_i + \breve{q}_i$. The error signal $\breve{q}_i$ is caused by the use of low-pass-filtered derivatives in Eq. (15).

Remark 3:

1) τ_d and τ_f are time constants of low-pass filters used to obtain biproper transfer functions in Eqs. (14) and (15) wherever a signal derivative is used. As noted in Sec. III.A, such constants act as tuning parameters that contribute to speed up fault detection, although at the expense of an increased sensitivity to measurement noise.

2) Eq. (14) is similar to Eq. (6) in Sec. III.A; that is $\hat{x}_j$ and $\hat{y}_j$ are signals that are exogenous to vehicle i. Such signals are obtained by using the filtered inversion of the nominal model of i, which corresponds to Eq. (1), valued at A^*_i and B^*_i.

3) The linear observer in Eq. (13) is composed of matrices $A_{F,i}$, $B_{F,i}$, and $C_{F,i}$, which are derived in the sequel to minimize the impact of $\hat{x}_j$ and $\hat{y}_j$, and of coupling terms $\hat{x}_j - x^*_{ij}$ and $\hat{y}_j - y^*_{ij}$. The coupling terms represent the interaction of vehicle i with its neighbors $j \in N_i$.

Instrumental in obtaining conditions on the observer's matrices, an augmented estimation error system, which includes the faulty simplified model in Eq. (1), is derived.

First, note that the system expressed in Eq. (14) can be written as

$$\begin{aligned} B^*_i \hat{v}_{i1}(s) &= \dot{q}_i(s) - A^*_i q_i(s) - \dot{\breve{q}}_i(s) + A^*_i \breve{q}_i(s) + B^*_i v_{i2}(s) \\ &= \tilde{A}_i q_i(s) + B_i[v_{i1}(s) - v_{i2}(s)] + \delta_i(s) - \dot{\breve{q}}_i(s) \\ &\quad + A^*_i \breve{q}_i(s) + B^*_i v_{i2}(s) \end{aligned} \tag{16}$$

where the first equality is obtained by substituting for $\bar{q}_i + \breve{q}_i$ in Eq. (14). The second equality is obtained by replacing q_i with the simplified model given in Eq. (1), to which the faulty signal δ_i is added.

Then, letting

$$\begin{aligned} \alpha_{i2}(s) &= \frac{B_i v_{i1}(s) - \tilde{B}_i v_{i2}(s) - \dot{\breve{q}}_i(s) + A^*_i \breve{q}_i(s)}{\tau_f s + 1} \\ A'_i(\alpha) &= \begin{bmatrix} -1/\tau_f & 0 \\ 0 & A_i(\alpha) \end{bmatrix}, \qquad \tilde{A}'_i(\alpha) = [\,\tilde{A}_i(\alpha) \quad 0\,] \\ B'(\alpha) &= \begin{bmatrix} 0 \\ B_i(\alpha) \end{bmatrix}, \qquad C'_i = [\,0 \quad C_i\,], \qquad Q_i = \begin{bmatrix} \varsigma_{1i} \\ q_i \end{bmatrix} \\ \dot{\varsigma}_{2i} &= (\delta - \varsigma_{2i})/\tau_f, \qquad \Delta_i = [\,\delta_i \quad \varsigma_{2i}\,]^T \end{aligned} \tag{17}$$

where state-space variables ς_{1i} and ς_{2i} result from the realization of the filter $1/(\tau_f s + 1)$ used in Eq. (14) and from the filtering of δ_i, respectively, which yields the following augmented estimation system:

$$\begin{aligned} \begin{bmatrix} \dot{Q}_i \\ \dot{\hat{q}}_i \end{bmatrix} &= \underbrace{\begin{bmatrix} A'_i(\alpha) & 0 \\ B_{F,i}C' + \tilde{A}'(\alpha) & A_{F,i} \end{bmatrix}}_{\mathsf{A}_i(\alpha)} \begin{bmatrix} Q_i \\ \hat{q}_i \end{bmatrix} \\ &\quad + \underbrace{\begin{bmatrix} B'_i(\alpha) & 0 \\ 0 & I \end{bmatrix}}_{\mathsf{B}_i(\alpha)} \begin{bmatrix} v_{i1} - v_{i2} \\ \alpha_{i2} \end{bmatrix} + \begin{bmatrix} \begin{bmatrix} 0 \\ 1 \end{bmatrix} & 0 \\ 0 & 1 \end{bmatrix} \Delta_i \\ z &= [\,C'_i \quad -C_{F,i}\,] \begin{bmatrix} Q_i \\ \hat{q}_i \end{bmatrix} \end{aligned} \tag{18}$$

where the equation for the derivative of $\hat{q}_i$ is obtained 1) by substituting the right-hand side of the second equality in Eq. (16) for $B^*_i \hat{v}_{i1}(s)$ in Eq. (13), 2) by using $B^*_i = B_i - \tilde{B}_i$, and 3) by noticing that $B_i v_{i2}(s)$ cancels out. The equation for the derivative of Q_i comes from Eq. (1) augmented with ς_{1i}.

In the case of a Luenberger-type observer ($A_{F,i} = A^*_i$ and $C_{F,i} = C_i$), the residue z can be expressed as

$$\begin{aligned} z(s) &= \underbrace{C'_i(sI - A^{*'}_i)^{-1}}_{H_1(s)} \tilde{A}_i Q_i(s) \\ &\quad + \underbrace{C'_i(sI - A^{*'}_i)^{-1} B'_i(\alpha)[v_{i1}(s) - v_{i2}(s)] - C_i(sI - A^{*'}_i)^{-1}\alpha_{i2}(s)}_{H_2(s)} \\ &\quad - \underbrace{C_i(sI - A^{*'}_i)^{-1}\frac{\tau_f s}{\tau_f s + 1}}_{G_i}\delta(s) \end{aligned} \tag{19}$$

where $A^{*'}_i = A'_i(\alpha^*)$. G_i is similar to $H(s)\delta(s)$ in Eq. (7), that is, as a low-pass-filtered derivative of the faulty signal.

Attenuation of the impact of disturbance α_{i2} on residue z leads to the computation of the observer matrices $A_{F,i}$, $B_{F,i}$, and $C_{F,i}$, obtained by solving a L_2-gain minimization problem defined as

$$\min_{A_{F,i}, B_{F,i}, C_{F,i}} \{\gamma; \|T_{\alpha_{i2} z_i}\|_\infty < \gamma\} \tag{20}$$

where

$$T_{w_i z_i} = (A_i, B_i, [\,C'_i \quad -C_{F,i}\,], 0)$$

A sufficient condition to meet the minimization constraint $\|T_{\alpha_{i2} z_i}\|_\infty < \gamma$ is given by the following matrix inequality:

$$\begin{bmatrix} P\mathsf{A}_i(\alpha) + \mathsf{A}^T_i(\alpha)P & P\mathsf{B}_i(\alpha) & [\,C'_i \quad -C_{F,i}\,]^T \\ \mathsf{B}^T_i(\alpha)P & -\gamma^2 I & 0 \\ [\,C'_i \quad -C_{F,i}\,] & 0 & -I \end{bmatrix} < 0 \tag{21}$$

which depends on a product of matrix variables such as $PB_{F,i}$.

Following the procedure of [10], it can be shown that Eq. (21) is equivalent for all $j \in \{1, \ldots, s\}$ to a linear matrix inequality (LMI) that can be efficiently solved by a numerical toolbox. Adopt the

following notation: $*$ stands for terms that are induced by symmetry in a matrix, $\Theta = [I \quad 0]^T$, $\mathcal{C}_j = \mathrm{diag}(C_i', I)$, and $\Im = [I \quad I]$.

Proposition 1: The observer given in Eqs. (13–15) characterized by matrices $A_{F,i}$, $B_{F,i}$, and $C_{F,i}$ satisfies the robust estimation constraint $\|T_{\alpha_{i2}z_i}\|_\infty < \gamma$ whenever there exists $\mu_i > 0$ such that the following LMI

$$\begin{bmatrix} -\mu_i(\hat{V}_i + \hat{V}_i^T) & \hat{V}_i^T\Theta A_{ij}\Theta^T + \Im^T\hat{K}_i\mathcal{C}_j + \Im^T\tilde{A}_{ij}\Theta^T + \hat{X}_i^T & \hat{V}_i^T\Theta B_{ij} & 0 & \mu_i\hat{V}_i^T \\ * & -\hat{X}_i & 0 & \begin{bmatrix} C_i'^T \\ -\hat{C}_{F,i}^T \end{bmatrix} & 0 \\ * & * & -\gamma^2 I & 0 & 0 \\ * & * & * & -I & 0 \\ * & * & * & * & -\hat{X}_i \end{bmatrix} < 0 \tag{22}$$

is feasible for all A_{ij} and B_{ij} with $j \in \{1, \ldots, s\}$ in

$$\hat{V}_i = \begin{bmatrix} \hat{V}_{1,i} & \hat{V}_{2,i} \\ \hat{V}_{3,i} & \hat{V}_{3,i} \end{bmatrix}$$

$\hat{X}_i$, $C_{F,i}$, and $\hat{K}_i$. The observer matrices are expressed as $A_{F,i} = \hat{A}_{F,i}\hat{V}_{3,i}^{-T}$, $B_{F,i} = \hat{B}_{F,i}$, and $C_{F,i} = \hat{C}_{F,i}\hat{V}_{3,i}^{-T}$.

Proof: The proof is similar to that of Theorem 5 in [10] applied to Eq. (18) and to Eq. (21) and by noticing that the extra coupling term $\tilde{A}_i'(\alpha)$ in $\mathsf{A}_i(\alpha)$, which is not present in Theorem 5 of [10], yields $\Im^T\tilde{A}_{ij}\Theta^T$, located in the 1×2 entry of Eq. (22). This product comes from $\Gamma\tilde{A}_{ij}\Theta^T$, which is part of $\mathsf{A}_i(\alpha)$ that can be expressed as

$$\mathsf{A}_i(\alpha) = \sum_{j=1}^{s} \alpha_{ij}(\Theta A_{ij}\Theta^T + \Gamma K_i\mathcal{C}_j + \Gamma\tilde{A}_{ij}\Theta^T) \tag{23}$$

where $\Gamma = [0 \quad I]^T$, and $K_i = [B_{F,i} \quad A_{F,i}]$. To obtain LMI in Eq. (22), the congruence transforms $\mathrm{diag}(\Pi_{V_i}, \Pi_{V_i}, I, I, \Pi_{V_i})$, where

$$\Pi_{V_i} = \begin{bmatrix} I & 0 \\ 0 & V_{22,i}^{-1}V_{21,i} \end{bmatrix}$$

$$V_i = \begin{bmatrix} V_{11,i} & V_{12,i} \\ V_{21,i} & V_{22,i} \end{bmatrix} = \begin{bmatrix} \hat{V}_{1,i} & \hat{V}_{2,i}\hat{V}_{3,i}^{-T} \\ I & \hat{V}_{3,i}^{-T} \end{bmatrix}$$

is first applied to Eq. (B2), described in Appendix B. Note that Eq. (B2) is applied to Eq. (21) and uses Eq. (23). Then, the following useful relationships are employed:

$$\Pi_{V_i}\Theta A_{ij}^T\Theta^T V_i\Pi_{V_i} = \Theta A_{ij}^T\Theta^T\hat{V}_i$$

$$\Pi_{V_i}^T C_j^T K_i^T\Gamma^T V_i\Pi_{V_i} = C_j^T\hat{K}_i^T\Im$$

and

$$B_{ij}^T\Theta^T V_i\Pi_{V_i} = B_{ij}^T\Theta^T\hat{V}_i$$

As already noticed, the congruence transform yields the extra term

$$\Pi_{V_i}^T\Theta^T\tilde{A}_{ij}\Gamma^T V_i\Pi_{V_i}$$

which can be shown to be equal to $\Theta\tilde{A}_{ij}^T\Im$ by noticing that

$$\Gamma^T V_i\Pi_{V_i} = V_{21,i}\Im = \Im$$

and that $\Pi_{V_i}^T\Theta = \Theta$. □

C. Threshold Selection

The tracking error of each vehicle increases in norm as the leader-to-vehicle relative distance increases. In fact, constraining tracking errors within small bounds requires the formation to behave almost like a rigid body, which would entail prohibitively large transient control signals used for vehicles significantly remote from the leader [7]. Therefore, the minimum detectable fault and the corresponding threshold are expected to be functions of leader-to-vehicle relative distances and thus should be selected carefully. As mentioned for Eq. (9), to avoid false alarms, the threshold must be defined such that

$$\inf_{\delta\in\Omega, Q, v_{i1}, v_{i2}, \alpha_{i2}} \|z\|_\tau > \sup_{\delta=0, Q, v_{i1}, v_{i2}, \alpha_{i2}} \|z_i\|_\tau \tag{24}$$

From [9], Eq. (24) is satisfied if

$$\inf_{\delta\in\Omega} \|G_i(s)f_i(s)\|_\tau > 2 \sup_{Q, v_{i1}, v_{i2}, \alpha_{i2}} \|H_1(s)\tilde{A}_i(s)Q_i(s) + H_2(s)\|_\tau \tag{25}$$

As noted in Sec. III.A, the minimum detectable fault associated with vehicle i can be characterized by the following lower bound on D_i, introduced in Eq. (3):

$$|D_i| \geq \frac{2 \sup_{Q, v_{i1}, v_{i2}, \alpha_{i2}} [\|H_1(s)\tilde{A}_i(s)\|_\infty \|Q_i(s)\|_\tau + \|H_2(s)\|_\tau]}{\underline{\sigma}[\Lambda_{G_i(s)}(\tau - t_f)]} \tag{26}$$

where $\underline{\sigma}$ denotes the minimum singular value of its argument. Because $G_i(s)$ is a matrix, $\Lambda_{G_i(s)}(\tau - t_f)$ in Eq. (26) is defined as the following matrix operator:

$$\sqrt{1/\tau \int_0^\tau [L^{-1}\{G_i(s)/s\}]^T L^{-1}\{G_i(s)/s\}\, \mathrm{d}t}$$

It is shown in [7] that the Euclidean norm of position and speed tracking errors of vehicle i is an increasing function of the relative distance ρ_{oi}^* between the leader and follower i, from which the bound

$$\|Q_i\|_\tau \leq \|Q_i\|_2 \leq [a_{i1} + \varphi_{i1}(\rho_{\mathrm{oi}}^*)]/2$$

can be derived, where $a_{i1} > 0$, and φ_{i1} is an increasing function. Thus, a sufficient condition for the detection of a fault δ_i can be expressed as

$$|D_i| \geq \frac{J_{\mathrm{th},i}}{\underline{\sigma}[\Lambda_{G_i(s)}(\tau - t_f)]} \tag{27}$$

where

$$J_{\mathrm{th},i} \geq [a_{i1} + \varphi_{i1}(\rho_{\mathrm{oi}}^*)]\|H_1(s)\tilde{A}_i(s)\|_\infty + \|H_2(s)\|_\tau$$

Inequality (27) shows that false alarms are avoided by increasing $J_{\mathrm{th},i}$, which in turn may impede fault detection of vehicles for which the distances from the leader are significantly larger than those of the leader's neighbors.

IV. Experiments and Simulations

A string of nine regularly spaced and aligned vehicles, $\{1, \ldots, 9\}$, is considered, where 1 and 9 denote the leader and the last follower vehicle of the string, respectively. Neighboring set N_i is defined for all $i \in \{2, \ldots, 9\}$ as $N_i = \{i-1\}$. As depicted in Fig. 4, the leader of the formation tracks a square trajectory with a side length of 100 m at a speed of 1 m/s. Followers are required to stabilize around the commands $\rho^* = 1$ m and $\lambda^* = 0$ rad. However, follower trajectories are not constrained beyond the stabilization requirement. The latter implies that obstacle/collision avoidance has to be implemented onboard or that the trajectory of the leader has to be planned so as to compensate for unacceptable transient deviations that may occur between follower and leader trajectories. This topic is outside the scope of the present work.

Hardover failure of a single actuator occurs at the time of fault $t_f = 150$ s onboard vehicles 2 and 6; that is, the actuators saturate at 3.5 N, and so one has from Eqs. (2) and (3)

$$\delta_i = 1_{t-t_f}\{H_{\mathrm{OF},t-t_f}[F_{\mathrm{in}}(t)] - F_{\mathrm{in}}(t)\}$$
$$H_{\mathrm{OF},t-t_f}(x) = \begin{cases} x, & \text{if } t - t_f < 0 \\ 3.5 \text{ N}, & \text{otherwise} \end{cases} \tag{28}$$

Modeling of the ALTAVs and of the instrumentation parameters is obtained from experimental data, as described in Appendix A. The six-degree-of-freedom model in a closed loop with multiloop proportional–integral-derivative (PID) autopilot is used for the simulations. Autopilots and distributed controllers in Appendix A and observers in Eqs. (13–15) are discretized (Runge–Kutta) with a sampling period of 10 ms.

The simplified model in Eq. (1), which is derived to provide trajectories sufficiently close to those of each ALTAV $i \in \{1, \ldots, 9\}$ of the formation, as described in Appendix A, is characterized by $\alpha_i = [\omega_i, \xi_i]$:

$$A_i(\alpha_i) = \begin{bmatrix} A_{\mathrm{di}}(\alpha_i) & 0_2 & 0_2 \\ 0_2 & A_{\mathrm{di}}(\alpha_i) & 0_2 \\ A_{31i}(\alpha_i) & A_{32i}(\alpha_i) & A_{\mathrm{di}}(\alpha_i) \end{bmatrix}$$
$$A_{\mathrm{di}}(\alpha_i) = \begin{bmatrix} 0 & 1 \\ -\omega_i^2 & -2\xi_i\omega_i \end{bmatrix}, \qquad A_{31i}(\alpha_i) = \begin{bmatrix} 0 & 0 \\ 0 & a_1 \end{bmatrix}$$
$$A_{32i}(\alpha_i) = \begin{bmatrix} 0 & 0 \\ 0 & a_2 \end{bmatrix}$$

$B_i(\alpha_i) = \mathrm{diag}[B_{\mathrm{di}}(\alpha_i), B_{\mathrm{di}}(\alpha_i), B_{\mathrm{di}}(\alpha_i)]$ and $B_{\mathrm{di}}^T(\alpha_i) = [0, \omega_i^2]$, along with the following parameter values $\omega_1 = 0.65$ rad/s, $\xi_1 = 0.32$, $\omega_2 = \omega_3 = 0.35$ rad/s, $\xi_2 = \xi_3 = 0.8$, $\omega_4 = 0.39$ rad/s, $\xi_4 = 0.89$, $\omega_5 = \omega_6 = 0.33$ rad/s, $\xi_5 = \xi_6 = 0.9$, $\omega_7 = \omega_8 = 0.35$ rad/s, $\xi_7 = \xi_8 = 1$, $\omega_8 = 0.33$ rad/s, $\xi_8 = 1$, $a_1 = -0.035$, and $a_2 = 0.01$.

The single robust observer used in the DFD and implemented onboard each ALTAV is designed from a single pair of polytopic matrices A_i and B_i that allows state-space matrices to encompass ALTAVs 2 to 8. To this purpose, we can exploit the fact that parameters α_i ($i \in \{2, \ldots, 8\}$) of vehicles 2 to 8 can be bounded by $\omega^* \pm \tilde{\omega}^M$ and $\xi^* \pm \tilde{\xi}^M$, where $\omega^* = 0.35$ and $\xi^* = 0.85$. The maximal deviations $\tilde{\omega}^M$and $\tilde{\xi}^M$are equal to 20% of the nominal values. The observer matrices in Eq. (13) are computed by means of the Matlab Robust Control Toolbox. Robust estimation is achieved with an attenuation gain $\gamma = 0.8$ and with $\mu_i = 1$. The following matrices are thus calculated: $A_{F,i} = \mathrm{diag}(a_{F,i}, a_{F,i})$, $B_{F,i} = \mathrm{diag}(b_{F,i}, b_{F,i})$, and $C_{F,i} = \mathrm{diag}(c_{F,i}, c_{F,i})$, where

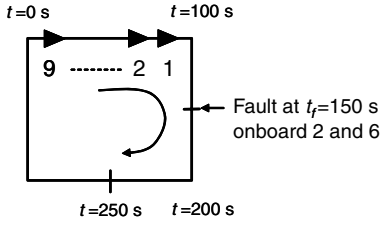

Fig. 4 Trajectory of the leader from $t = 0$ to 250 s.

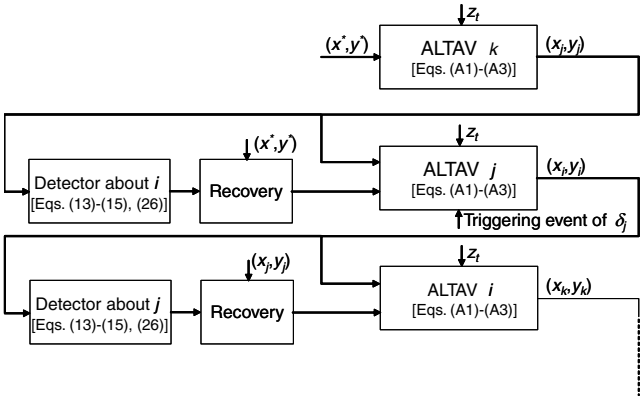

Fig. 5 Distributedly controlled formation of ALTAVs equipped with their DFD and recovery module.

$$a_{F,i} = \begin{bmatrix} -2.56 & 0.95 \\ -0.14 & -0.84 \end{bmatrix}$$

$b_{F,i} = 10^{-2}[-3.85, -0.76]^T$, and $c_{F,i} = [-89.85, 9.64]^T$. The time window used to compute the rms error is $\tau = 1$ s. The thresholds described in Sec. III are selected as $J_{\mathrm{th},3} = J_{\mathrm{th},4} = J_{\mathrm{th},5} = 0.12$, $J_{\mathrm{th},6} = J_{\mathrm{th},7} = 0.125$, and $J_{\mathrm{th},8} = J_{\mathrm{th},9} = 0.13$. The inverse dynamics and derivatives are filtered with a first-order, low-pass filter for which the time constants are $\tau_f = 5$ s and $\tau_d = 0.05$ s, respectively.

The guidance adaptation, denoted as recovery in Fig. 5, is implemented onboard each vehicle as follows: when a fault is detected on the upstream faulted neighbors k-1, by means of the DFD design, vehicle k establishes a link with vehicle k-2, assumed in range, by means of its onboard sensors. The detector flag of fault occurrence is triggered as soon as $\|r_{ix}\|_\tau = \|C_{ix}z_i\|_\tau \geq J_{\mathrm{th},i}$ or $\|r_{iy}\|_\tau = \|C_{iy}z_i\|_\tau \geq J_{\mathrm{th},i}$ (where $C_{ix} = [1 \quad 0]$ and $C_{iy} = [0 \quad 1]$) is satisfied. Simulations displayed in the sequel implement the block diagram in Fig. 5 for the first three ALTAVs.

The simulations aim at verifying that

1) The transients induced by corner following do not induce false alarms.

2) Vehicles 3 and 7 detect faults of vehicles 2 and 6 with the same robust observer, which accounts for parametric uncertainty that arises from the simplified formation modeling used to design the observer.

3) The transient behavior of the formation over $[t_f, \tau + t_f)$ does not induce false alarms in vehicles 4, 5, 8, and 9.

Figure 6 shows that large residues appear only after the fault occurrence and that tracking error caused by turning around the corner at $t = 100$ s does not provide false alarms. Faults in vehicles 2 and 6 are detected after a delay of 4 and 9 s, respectively.

Planar trajectories of faulted vehicles 2 and 6 and their adjacent neighbors are shown in Fig. 7. One can notice that fault detection by vehicles 3 and 7 is sufficiently fast enough for all of the vehicles except 2 and 6 to continue following the leader.

Snapshots of the formation in motion are depicted in Fig. 8. The integrity of the formation composed of all the vehicles except 2 and 6 is preserved, because the anomalous behavior of the two diverging vehicles is detected sufficiently fast and acted upon quickly. The formation does not, however, maintain its original aspect in terms of relative distances ρ_{ij}^* between adjacent neighbors. The vehicles are close to their maximum allowable speed in a straight line and thus cannot reduce the intervehicle distances that have been abruptly increased by the detection of faulty vehicles 2 and 6. Nevertheless, a slight crossing of the corner at $t = 260$ s, as depicted in Fig. 8d, allows the formation, exempt of vehicles 2 and 6, to stabilize around the prescribed ρ_{ij}^*. The simulation results also demonstrate that the approach that consists of using the same robust observer onboard each ALTAV's detector enabled the detection of concurrent faults, although ALTAV closed-loop dynamics depend on their position in the formation.

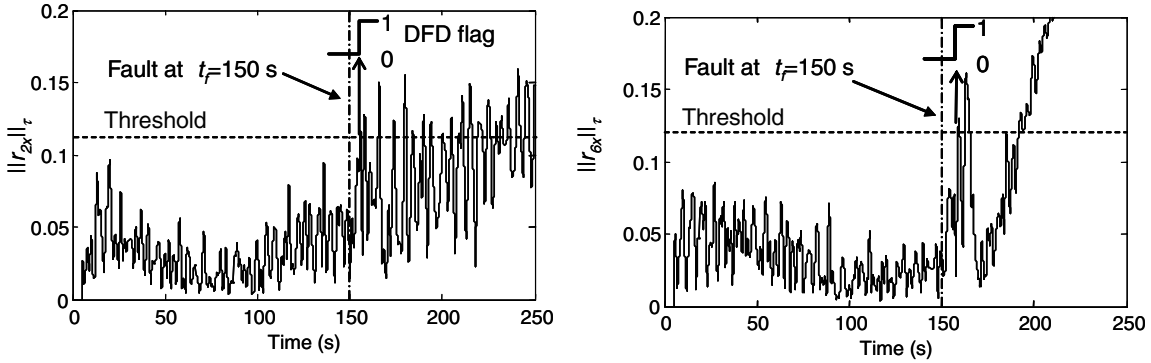

Fig. 6 Residues in the x axis about the abnormal operating condition of vehicles 2 and 6 computed by vehicles 3 (left) and 7 (right).

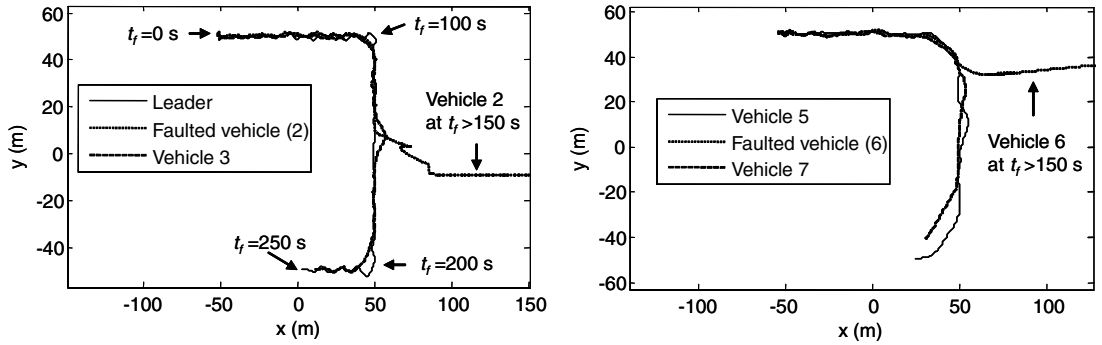

a) Vehicles 1, 2, and 3 **b) Vehicles 5, 6, and 7**

Fig. 7 Planar trajectories of faulty vehicles and adjacent neighbors when the leader follows a square trajectory.

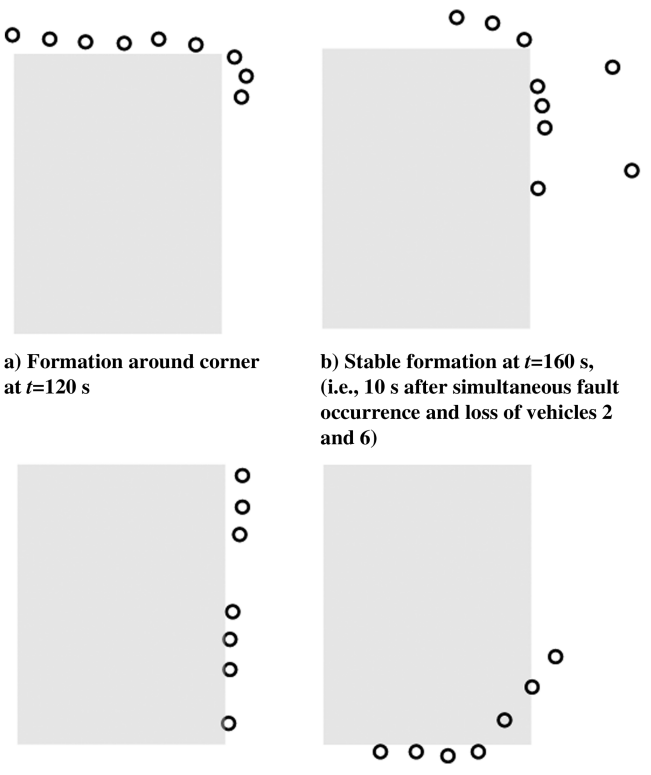

a) Formation around corner at t=120 s

b) Stable formation at t=160 s, (i.e., 10 s after simultaneous fault occurrence and loss of vehicles 2 and 6)

c) Formation stabilization at t=175 s with larger intervehicle distances (vehicles 2 and 6 excluded)

d) At t=260 s, intervehicle distances approach their prescribed values

Fig. 8 Snapshots of formation motion.

V. Conclusions

Decentralized fault detection for leader-to-follower formations based on local information was proposed. The scheme implemented enables detection of severe faults that remain uncompensated for by component-level FDIR. The detection relies on a mixed H_∞ minimization-based observer and on the compensation of exogenous unknown disturbances. The observer uses a simplified, uncertain, linearly parameterized model of the UAV dynamics in closed loop with the controllers. Simulation results show that the detection of concurrent faults and the subsequent adaptation can be achieved sufficiently fast to preserve formation cohesiveness. Future work includes live testing of the proposed DFD scheme and porting the algorithms to other types of unmanned vehicles.

Appendix A: ALTAV Closed-Loop Dynamics

The dynamics of the ALTAV is governed for all $i \in S$ by the following model [11]:

$$M\ddot{x}_i = \sum_j F_{ji}\sin(\gamma_i) - C_x\dot{x}_i, \qquad M\ddot{y}_i = \sum_j F_{ji}\sin(\phi_i) - C_y\dot{y}_i$$

$$M\ddot{z}_i = -\sum_j F_{ji}\cos(\gamma_i)\cos(\phi_i) - F_B + F_g - C_z\dot{z}_i$$

$$J_\theta\ddot{\theta}_i = (F_{1i}l_1 - F_{2i}l_2 + F_{3i}l_3 - F_{4i}l_4)\sin(\rho_i) - C_\theta\dot{\theta}_i$$

$$J_\gamma\ddot{\gamma}_i = F_{1i}l_1 - F_{3i}l_3 - F_Bl_B\sin(\gamma_i) - C_\gamma\dot{\gamma}_i$$

$$J_\phi\ddot{\phi}_i = -F_{2i}l_2 + F_{4i}l_4 - F_Bl_B\sin(\phi_i) - C_\phi \tag{A1}$$

where x_i, y_i, and z_i are the vehicle translations; θ, ϕ, and γ are the vehicle rotation angles; M is the mass of each vehicle; J_ϕ, J_γ, and J_θ are the moments of inertia about the x, y, and z axes; F_g is the force due to gravity; F_B is the buoyant force resulting from the volume of helium in the vehicle; F_i is the force magnitude of the ith motor ($i \in \{1, 2, 3, 4\}$); l_i are the perpendicular distances between the

motors and the vehicle center of gravity $i \in \{1, 2, 3, 4\}$; C_i is the drag coefficient in the direction $i \in \{x, y, z, \theta, \phi, \gamma\}$, which serves as a damping term for the motion in that direction; and ρ is the angular offset from the vertical axis of the motor thrust vectors.

The flight control and guidance laws consist of a set of PID controllers. In each vehicle, the flight controllers provide commands to the four motors to maintain the specified elevation, yaw, pitch, and roll and are expressed for all $i \in S$ as [11]

$$
\begin{aligned}
F_{1i} &= Sat_{0,S_F}(f_i + g_i + \lambda_i), \qquad F_{2i} = Sat_{0,S_F}(-h_i - g_i + \lambda_i)\\
F_{3i} &= Sat_{0,S_F}(-f_i + g_i + \lambda_i), \qquad F_{4i} = Sat_{0,S_F}(h_i - g_i + \lambda_i)\\
f_i &= p_{\varphi\gamma}(Sat_{-S_{\varphi\gamma},S_{\varphi\gamma}}(u_{xi}) - \gamma_i)\\
&\quad + i_{\varphi\gamma}\int_{t_i}^{t}(Sat_{-S_{\varphi\gamma},S_{\varphi\gamma}}(u_{xi}) - \gamma_i)d\upsilon - d_{\varphi\gamma}\dot{\gamma}_i\\
h_i &= p_{\varphi\gamma}(Sat_{-S_{\varphi\gamma},S_{\varphi\gamma}}(u_{xi}) - \varphi_i)\\
&\quad + i_{\varphi\gamma}\int_{t_i}^{t}(Sat_{-S_{\varphi\gamma},S_{\varphi\gamma}}(u_{xi}) - \varphi_i)d\upsilon - d_{\varphi\gamma}\dot{\varphi}_i\\
g_i &= p_\theta(u_{xi} - \varphi_i) + i_\theta\int_{t_i}^{t}(u_{xi} - \varphi_i)d\upsilon - d_\theta\dot{\varphi}_i\\
\lambda_i &= p_z(z_i - z_t) + i_z\int_{t_i}^{t}(z_i - z_t)d\upsilon + d_z(\dot{z}_i - \dot{z}_t)
\end{aligned}
\tag{A2}
$$

where the actuator's saturation function $Sat_{a,b}(x)$ is equal to x whenever $a \le x \le b$, equal to b whenever $x > b$, and equal to a in the remaining case. The flight controllers also generate pitch and roll commands u_x and u_y to move the vehicle in the x–y space. The outer-loop control of the leader of the formation, which is characterized by Cartesian state (x_o, y_o, z_o), is [11]

$$
u_{xo} = k_p(x^* - x_o) - k_d\dot{x}_o, \qquad u_{yo} = k_p(y^* - y_o) - k_d\dot{y}_o \tag{A3}
$$

where x^* and y^* stand for the reference trajectory to follow. Guidance for the follower $i \in S\{0\}$ with state (x_i, y_i, z_i) is given as [7]

$$
\begin{aligned}
[\,u_{xi} \quad u_{yi}\,]^T &= h_i\left(\sum_{j\in N_i} k_i[x_j - x_i - x_{ij}^* | y_j - y_i - y_{ij}^*]^T\right)\\
[\,x_{ij}^* \quad y_{ij}^*\,]^T &= \rho_{ij}^*[\cos(\lambda_{ij}^* + \psi_i)\sin(\lambda_{ij}^* + \psi_i)]^T
\end{aligned}
\tag{A4}
$$

where h_i is a strict positive real operator for which the stabilizability property is analyzed in [7], and h_i is selected as a low-pass-filtered PD controller, given as $\kappa_i(k_{p_i} + k_{s_i}s)/(1 + \tau_i s)$. The distributed controllers stabilize the formation in the x–y plane, whereas set-point regulation in z, given in Eq. (A2), is obtained by PID control around a prescribed altitude z_t, which is assumed to be known by the vehicles of the formation before the mission onset or command changes.

The following parameters are used in the simulations: $F_b = 13$ N, $M = 1.618$ kg, $J_t = .995$ kg · m^2, $J_\gamma = 1.005$ kg · m^2, $J_\phi = 1.005$ kg · m^2, $l_1 = .941$ m, $l_2 = .941$ m, $l_3 = .941$ m, $l_4 = .941$ m, $l_b = .16$ m, $g = 9.8$ m/s^2, $C_x = 0.95$, $C_y = 0.95$, $C_z = 0.95$, $C_t = 0.5$, $C_g = 0.5$, and $C_p = 0.5$.

Sensor measurements are corrupted by zero-mean white Gaussian noise. Noise variance and sensor sampling periods are given in Table 1.

Controller gains in Eqs. (A2–A4) are $p_z = 0.6$, $i_z = 0.2$, $d_z = 5$, $p_z = 0.125$, $p_\theta = 1$, $i_\theta = 0$, $d_\theta = 3$, $p_\theta = 0.125$, $i_\theta = 0.1$, $d_\theta = 2.5$, $p_z = 0.6$, $i_z = 0.2$, $d_z = 5$, $k_p = 0.5$, $k_i = 0$, $k_d = 0.7$, $S_{\varphi\gamma} = 0.69$ rad, $S_F = 3.5$ N, $\kappa_1 = 0.4$, $\kappa_2 = \kappa_3 = 0.3$, $\kappa_4 = 0.25$, $\kappa_5 = \kappa_6 = 0.23$, $\kappa_7 = \kappa_8 = 0.21$, $\kappa_9 = 0.2$, and $\tau_I = 0.05$ s.

Appendix B: Results of LMIs Applied to Uncertain Systems

The following result, taken from [10], is useful to obtain the linearization of matrix-inequality-based problems such as L_2-gain minimization, in which the Lyapunov variable is multiplied by a design variable.

Table 1 Sensor characteristics

Sensor	Noise variance	Sampling period, s
Global positioning system	1 m^2	1
Sonar	2 cm^2	1/50
Tilt	0.0349 rad^2	1/100
Compass	0.0349 rad^2	1/50

Theorem 1 [10]. The LMI

$$
X > 0, \qquad \begin{bmatrix} A^TX + XA & XB & C^T \\ B^TX & Q_{11} & Q_{12} \\ C & Q_{12}^T & Q_{22} \end{bmatrix} < 0 \tag{B1}
$$

is feasible in the decision variable X if, and only if, there is scalar $\mu > 0$ such that the following LMI

$$
\begin{bmatrix} -\mu(V + V^T) & V^TA + X & V^TB & 0 & \mu V^T \\ A^TV + X & -X & 0 & C^T & 0 \\ B^TV & 0 & Q_{11} & Q_{12} & 0 \\ 0 & C & Q_{12}^T & Q_{22} & 0 \\ \mu V & 0 & 0 & 0 & -X \end{bmatrix} < 0 \tag{B2}
$$

is feasible in the decision variables X, V, and V_1.

Other LMIs such as Eq. (B2) are provided in [10]. We retain the LMI that is useful to our purpose. From Eqs. (21) and (B1), one has $C = \lfloor\, C_i' \quad -C_{F,i}\,\rfloor$, $Q_{12} = 0$, $Q_{11} = -\gamma^2 I$, and $Q_{22} = -I$.

Acknowledgments

This work was partly funded by Defence Research and Development Canada and the Natural Sciences and Engineering Research Council of Canada.

References

[1] Boskovic, J. D., Bergstrom, S. E., and Mehra, R. K., "Robust Integrated Control Design Under Failures, Damage, and State-Dependant Disturbances," *Journal of Guidance, Control, and Dynamics*, Vol. 28, No. 5, 2005, pp. 902–917.

[2] Giulietti, F., Pollini, L., and Innocenti, M., "Autonomous Formation Flight," *IEEE Control Systems Magazine*, Vol. 20, No. 6, Dec. 2000, pp. 34–44.

[3] Pollini, L., Giulietti, F., and Innocenti, M., "Robustness to Communication Failures within Formation Flight," *Proceedings of the 2002 American Control Conference*, American Automatic Control Council, Evanston, IL, May 2002, pp. 2860–2866.

[4] Innocenti, M., and Pollini, L., "Management of Communication Failures in Formation Flight," *Journal of Aerospace Computing, Information, and Communication*, Vol. 1, No. 1, Jan. 2004, pp. 19–35.

[5] Mehra, R. K., Boskovic, J. D., and Li, S.-M., "Autonomous Formation Flying of Multiple UCAVS Under Communication Failure," *IEEE 2000 Position Location and Navigation Symposium*, Inst. of Electrical and Electronics Engineers, Piscataway, NJ, 2000, pp. 371–378.

[6] Léchevin, N., Rabbath, C. A., and Sicard, P., "Stable Morphing of Unicycle Formations in Translational Motion," *Proceedings of the 2006 American Control Conference*, Inst. of Electrical and Electronics Engineers, Piscataway, NJ, 2006, pp. 4231–4236.

[7] Léchevin, N., Rabbath, C. A., and Sicard, P., "Trajectory Tracking of Leader-Follower Formations Characterized by Constant Line-of-Sight Angles," *Automatica*, Vol. 42, Dec. 2006, pp. 2131–2141.

[8] Liang, F., Wang, J. L., and Yang, G.-H., "Reliable Robust Flight Tracking Control: An LMI Approach," *IEEE Transactions on Control Systems Technology*, Vol. 1, No. 1, 2002, pp. 76–89.

[9] Emami-Naeini, A., Akhter, M. M., and Rock, S. M., "Effect of Model Uncertainty on Failure Detection: The Threshold Selector," *IEEE Transactions on Automatic Control*, Vol. 33, No. 12, 1988, pp. 1106–1115.

[10] Tuan, H. D., Apkarian, P., and Nguyen, T. Q., "Robust Filtering for Uncertain Nonlinearly Parameterized Plants," *IEEE Transactions on Signal Processing*, Vol. 51, No. 7, 2005, pp. 1806–1815.

[11] Earon, E., "Almost-Lighter-Than-Air Vehicle Fleet Simulation," Quanser Inc., TR V.1.1, Toronto, Canada, 2006.